Light-Responsive Elastin-Like Peptide-Based Targeted Nanoparticles for Enhanced Spheroid Penetration.

Duc H T Le, Vusala Ibrahimova, Sebastian a H van den Wildenberg, Hanglong Wu, Alba Fonseca, Tomas Torres, Elisabeth Garanger, William P J Leenders, Roland Brock, Sébastien Lecommandoux, et al.

How to cite:
doi.org/10.1002/anie.202300511

Nanoparticles

Light-Responsive Elastin-Like Peptide-Based Targeted Nanoparticles for Enhanced Spheroid Penetration

*Duc H. T. Le, Vusala Ibrahimova, Sebastian A. H. van den Wildenberg, Hanglong Wu, Alba Fonseca, Tomas Torres, Elisabeth Garanger, William P. J. Leenders, Roland Brock, Sébastien Lecommandoux, and Jan C. M. van Hest**

Abstract: We describe here a near infrared light-responsive elastin-like peptide (ELP)-based targeted nanoparticle (NP) that can rapidly switch its size from 120 to 25 nm upon photo-irradiation. Interestingly, the targeting function, which is crucial for effective cargo delivery, is preserved after transformation. The NPs are assembled from (targeted) diblock ELP micelles encapsulating photosensitizer TT1-monoblock ELP conjugates. Methionine residues in this monoblock are photo-oxidized by singlet oxygen generated from TT1, turning the ELPs hydrophilic and thus trigger NP dissociation. Phenylalanine residues from the diblocks then interact with TT1 via π-π stacking, inducing the re-formation of smaller NPs. Due to their small size and targeting function, the NPs penetrate deeper in spheroids and kill cancer cells more efficiently compared to the larger ones. This work could contribute to the design of "smart" nanomedicines with deeper penetration capacity for effective anticancer therapies.

Introduction

Nanoparticles (NPs) self-assembled from (bio-)macromolecules, while holding great potential for (targeted) nanomedicine, fail most of the time in translational trials.[1] One of the major hurdles is the limited tissue penetration of NPs due to the presence of complex biological barriers in the tumor microenvironment (TME) such as aberrant vascularization, dense extracellular matrix fibrosis and increased interstitial fluid pressure.[1] The current state-of-the-art NPs typically have average sizes of 100 nm or larger, which are favorable for longer circulation time and tumor accumulation.[2] However, this does not lead to improved therapeutic effects due to limited tissue penetration.[2] A new trend in nanovehicle development is to construct NPs that are responsive to endogenous stimuli such as low pH or enzymes in the TME for changing their size.[3,4] However, employing external stimuli such as light to induce a size change for improving tissue penetration has been underexplored.[4] Moreover, short-term irradiation triggering a rapid response might also benefit cargo release.

NIR light (650–900 nm) is a highly efficient stimulus offering precise spatiotemporal control. It is currently exploited in photodynamic therapy (PDT) as a non-invasive approach for anticancer treatment and is typically combined with chemotherapy or immunotherapy to achieve synergistic effects.[5] PDT requires delivery of non-toxic photosensitizers (PSs) to the treatment sites where, only upon photo-irradiation, they generate highly toxic reactive oxygen species (ROS), which damage targets via oxidation. Various designs of self-assembling polymers and peptides have been developed for PS delivery and recently also for triggered release, in most cases intracellularly. Wang et al. exploited micellar systems based on selenium-containing block copolymers encapsulating doxorubicin and the PS indocyanine green.[6] Following cellular uptake, the particles disassembled rapidly upon light irradiation, due to ROS-mediated oxidation of selenium and released co-encapsulated

[*] Dr. D. H. T. Le, S. A. H. van den Wildenberg, Dr. H. Wu, Prof. Dr. J. C. M. van Hest
Department of Biomedical Engineering, Institute for Complex Molecular Systems (ICMS), Eindhoven University of Technology
PO Box 513, 5600 MB Eindhoven (The Netherlands)
E-mail: J.C.M.v.Hest@tue.nl

Dr. D. H. T. Le, Dr. W. P. J. Leenders, Prof. Dr. R. Brock
Department of Medical BioScience, Radboud Institute for Molecular Life Sciences (RIMLS), Radboud University Medical Center
Geert Grooteplein 28, 6525 GA Nijmegen (The Netherlands)

Dr. V. Ibrahimova, Dr. E. Garanger, Prof. Dr. S. Lecommandoux
Université Bordeaux, CNRS, Bordeaux INP, LCPO, UMR 5629
33600 Pessac (France)

A. Fonseca, Prof. Dr. T. Torres
Departamento de Química Orgánica and Institute for Advanced Research in Chemical Sciences (IAdChem),
Universidad Autónoma de Madrid
28049 Madrid (Spain)

Prof. Dr. R. Brock
Department of Medical Biochemistry, College of Medicine,
Arabian Gulf University
Manama 293 (Kingdom of Bahrain)

doxorubicin. In another study, synthetic peptides were co-assembled with the porphyrin Ce6. The system also responded quickly to light irradiation and dissociated into both smaller micellar structures (≈85 nm) and fibrils (>700 nm in length),[7] enhancing tumor retention of cargos and showing high cell-killing capacity in vitro and in vivo. The sizes after transformation were, however, larger than optimal (<30 nm) for tissue penetration. Another approach to improve on therapeutic efficacy is the incorporation of a targeting function, as shown for example for PDT treatment.[8,9] Unfortunately, particle dissociation is often not compatible with targeting, as the latter function is lost when the particles are disassembled. Here we present a novel polypeptide-based NP system that includes (1) rapid light-responsiveness to dissociate into smaller clusters for enhanced tissue penetration and (2) targeted cellular delivery of PSs for highly efficient PDT. The system was designed in a way that the targeting function was preserved after dissociation, thereby overcoming some of the limitations of current stimulus-responsive (targeted) delivery systems.

Elastin-like polypeptides (ELPs) are a class of temperature-responsive biopolymers that can be produced in subgram scales per liter culture from *E. coli.* They are tailor-made polymers with a high degree of sequence control.[10] Sequence designs of ELPs are based on the pentapeptide (GXGVP) repeating motif from human elastin protein, where the guest residue X can be any amino acid except for proline. ELPs are routinely referred to as [A_xB_y-n], where A and B indicate the different guest residues, x and y are their corresponding ratios, and n is the total number of pentapeptide repeats. An intrinsic property of ELPs is that upon heating above a specific transition temperature corresponding to their cloud point T_{cp}, the polymers reversibly switch from soluble monomers (hydrophilic state) into insoluble coacervates (hydrophobic state).[11] Rational design using combinations of [A,B,x,y,n] allows precise control over T_{cp} and/or further endows the polypeptides with additional responsiveness to stimuli like pH or ions.[12,13] Recently, Ibrahimova et al. constructed a hydrophobic ELP [M_1V_3-40] with methionine (Met, M) and valine (Val, V) guest residues and conjugated it to TT1,[14] a NIR wavelength (650–660 nm) absorbing phthalocyanine-based PS with superior photophysical properties.[15,16] Upon light irradiation, the thioether groups from the Met side chains were photo-oxidized into sulfoxide groups by ROS generated from TT1.[14] As a result, the photo-oxidized ELP became more hydrophilic leading to a shift to a higher T_{cp}.[14,17] This light-responsive switch could thus be employed as a smart tool to control the disassembly of NPs. As [M_1V_3-40] by itself formed micron-sized coacervates rather than NPs, we employed the co-assembly approach described by Pille et al. to prepare homogeneous micellar NPs.[18] The co-assembly approach is a kinetic-driven pathway in which a mixture of an amphiphilic diblock (db) ELP and a monoblock (mb) ELP is rapidly heated above the T_{cp} of the hydrophobic block of dbELP and the T_{cp} of the mbELP. As a result, the mbELP is kinetically entrapped within the hydrophobic core of the micelles formed by the dbELP. Cargos, when conjugated with the mbELP, are co-encapsulated, allowing efficient loading in a one-step assembly.

In this work, we employed a dbELP with the sequence denoted as [A_3G_2-60]-[V_4F_1-50], which forms micelles above 28 °C (Figures S1 and S2), and the PS-mbELP conjugate TT1-[M_1V_3-40][14] for preparing co-assembled NPs. The guest residue phenylalanine (Phe, F) was introduced in the hydrophobic block [V_4F_1-50] for enhanced stability of the micelle's hydrophobic core via π-π stacking and to provide interaction with TT1. For targeting purposes, the anti-epidermal growth factor receptor (EGFR) nanobody 7D12[19] was selected as the targeting module and genetically fused to the N-terminus of the hydrophilic block [A_3G_2-60] of the dbELP (7D12-dbELP). This nanobody was previously employed in targeted ELP NP systems developed by our group for PDT applications.[8] The targeted NP has high affinity and is highly selective towards EGFR-positive cells, resulting in highly efficient PDT treatment.[8] After co-assembly, 7D12 moieties will be exposed and accessible for EGFR binding followed by NP internalization.[8,18] Upon light irradiation, photo-oxidation makes the encapsulated TT1-[M_1V_3-40] hydrophilic, triggering instability in the hydrophobic core and disassembly. The designed interaction between Phe residues and TT1 should however yield the formation of smaller clusters in which the nanobody and PS function are kept after transformation. The schematic of particle formation and the disassembly pathway upon light irradiation is shown in Scheme 1.

Results and Discussion

ELPs were synthesized in *E. coli* and purified using the established Inverse Transition Cycling method (Supporting Information). The co-assembled NPs were prepared by adding pre-heated PBS into the mixture of dbELP, TT1-mb ELP, and with or without 7D12-dbELP to induce rapid micelle formation and encapsulation of the conjugate. NP preparation is detailed in Supporting Information. First, dynamic light scattering (DLS) was used to determine the size and dispersity of the co-assembled NPs. As shown in Figures 1A and S3A, the co-assembled NPs had a hydrodynamic diameter of 117 ± 27 nm, with a polydispersity index (PDI) of 0.14, indicating a relatively monodispersed population. The targeted NPs also had a similar diameter of 124 ± 46 nm (PDI 0.19) (Figures 1B and S3B). Co-assembled NPs were significantly larger than NPs assembled from the dbELP alone (45 ± 15 nm, Figure S2). The TT1-mbELP conjugate itself only formed ill-defined micron-sized coacervates at 37 °C.[14] The combined data indicate that the TT1-mbELP conjugates were encapsulated within the dbELP during co-assembly. To study the light-responsiveness, a 660 nm laser light source (0.12 W cm^{-2}) was used to irradiate the particle suspension for 5 min, followed by DLS at 37 °C. Photo-irradiation led to a shift to smaller sizes for both non-targeted and targeted micelles, 25 ± 9 nm (PDI 0.12) and 25 ± 7 nm (PDI 0.21) respectively (Figures 1A, 1B, and S3). Photo-oxidation of encapsulated TT1-mbELP was further analyzed with denaturing gel electrophoresis SDS-PAGE in

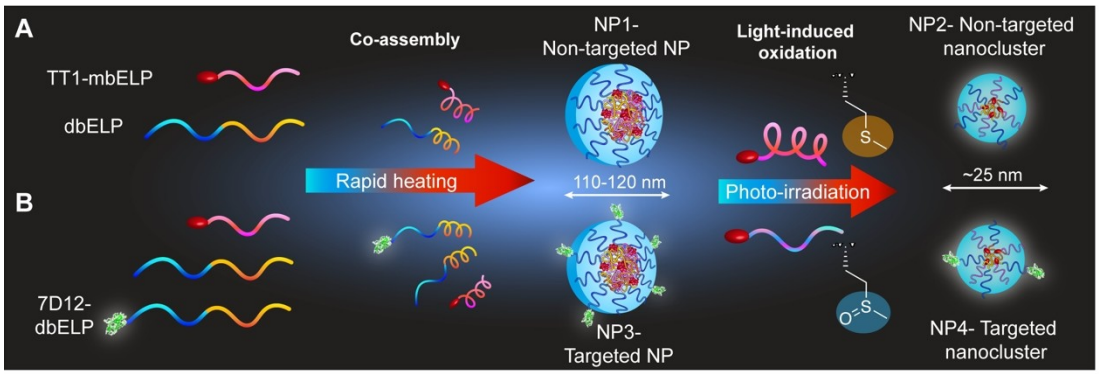

Scheme 1. Schematic of the formation of co-assembled NPs without (A) and with (B) the targeting ligand (EGFR-targeting nanobody 7D12). Upon light irradiation, the NPs rapidly disassemble because of photo-oxidation of the Met-containing monoblock ELP carrying the photosensitizer (TT1-mbELP), which is encapsulated within the NPs formed by the diblock (db) ELPs. The hydrophobicity-to-hydrophilicity shift induces disassembly, while π-π stacking of the TT1 photosensitizer with the Phe residues of the dbELP, including the 7D12 containing dbELP (7D12-dbELP), results in reorganization in smaller (targeted) nanoclusters.

which a molecular weight shift was observed of the fluorescent TT1-[M_1V_3-40] (Figure 1C). Similarly, a shift in elution of TT1-[M_1V_3-40] upon light treatment was detected (Figure 1D). Deconvoluted masses of these peaks indicated that five to seven thioethers of the in total eleven Met residues were oxidized (Figure S4 and Table S2). The photo-oxidized TT1-mbELP, with a higher T_{cp}, became more hydrophilic,[14] which triggered instability and disassembly of the co-assembled NPs. Hereafter, the non-targeted and targeted NPs without light treatment are named NP1 and 3, respectively. After light irradiation, NP1 and 3 were converted into non-targeted NP2 and targeted NP4, respectively.

The morphologies of these NPs were further confirmed by cryogenic transmission electron microscopy (cryo-TEM). As shown in Figure 1E, NP1 had a spherical morphology with the size ranging from 80–110 nm. Due to temperature fluctuations and the presence of ambient light during sample preparation for imaging, the observed particle sizes might be affected and appeared to be more polydisperse. Multiple black dots were also observed within the NP; this higher electron density could be attributed to the stacking of multiple TT1 bearing zinc atoms. Given that the hydrophobic block contains multiple Phe guest residues, there might be also interaction with TT1 via π-π stacking. Upon light irradiation, significantly smaller-sized protein clusters (NP2) were observed, with a size of approximately 10 nm (Figures 1E and S5). Because cryo-TEM only reflected the condensed hydrophobic core, this might explain the smaller size compared to DLS measurements. The morphologies looked homogeneous even though they consisted out of multiple ELP species. Moreover, they were also different from micelles assembled from dbELP alone which have a larger hydrophobic core as seen in our previous work.[13] These findings strongly suggest that the clusters were composed of both dbELP and photo-oxidized TT1-mbELP. The hydrophilic region was now extended to both the [A_3G_2-60] domain from the dbELP and the oxidized [M_1V_3-40] domain, both of which played a role in colloid stabilization (Scheme 1). The two ELPs were kept together through π-π stacking between the Phe residues and TT1. Overall, DLS and cryo-TEM results together confirmed the formation of NPs using the co-assembly method and their re-organization upon photo-irradiation. The targeted NP3 and the targeted nanoclusters (NP4) showed similar characteristics, and no differences were observed with cryo-TEM (Figures 1E and S5) and DLS measurements (Figures 1A and 1B) compared to NP1 and 2, respectively. Furthermore, UV/Vis spectroscopy also did not show differences between ELP NP1–4; all had a broad absorbance between 600–700 nm with the peak at 630 nm, indicative of the presence of TT1 (Figure S6). The nanoclusters were expected to also contain the nanobody, as 7D12 was conjugated to the same Phe residues-containing dbELP. This would endow the nanoclusters with a targeting function. To unambiguously demonstrate its presence, cell uptake studies were performed.

We thus investigated the interaction of NP1–4 with the EGFR-expressing human carcinoma cell line A431[20] to study their targeting functions. The uptake pathways of the NPs were monitored spectroscopically via TT1 fluorescence (Ex/Em 630/660 nm), which was conjugated to the mbELP, and via Cy3 fluorescence (Ex/Em 550/580 nm) attached to the N-terminus of the dbELP. After incubation for 1.5–3 hours, cells were washed and imaged live using confocal microscopy. Uptake of the targeted NP3 was already observed within 1.5 hours while there was no signal observed for NP1 up to 3 hours (Figures S7 and 2A). The punctate intracellular signals suggest that NP3 was endocytosed. The Pearson's coefficients of TT1 and Cy3 from NP3 after 1.5 and 3 hours were 0.80 and 0.78, respectively, indicating the presence of intact NPs. We then sought to explore the behavior of the nanoclusters toward cell uptake, and especially to learn whether the targeting function was preserved. Similar to NP1, NP2 did not show uptake after 1.5 and 3.0 hours (Figures S7 and 2A). In the case of NP4, the signals of Cy3 and TT1 were detected in both time points (Figures S7 and 2A). Because only 10 % dbELP was

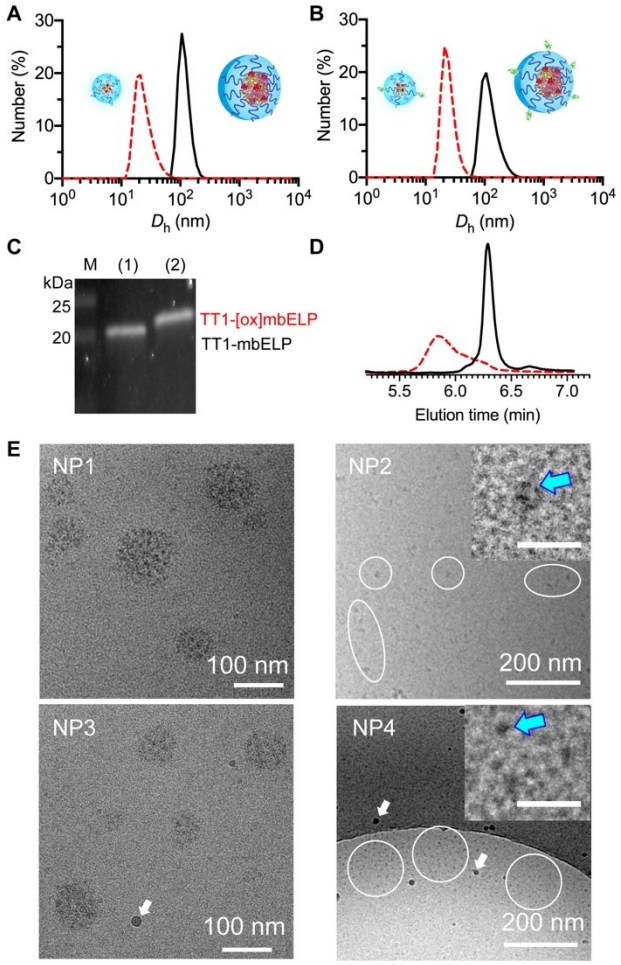

Figure 1. Characterization of ELP NPs. DLS profiles of (A) non-targeted NPs before (NP1-black line) and after light irradiation (NP2-red dotted line), and (B) targeted NPs before (NP3) and after light irradiation (NP4). (C) SDS-PAGE of TT1-mbELP encapsulated within the co-assembled NP before (1) and after (2) light irradiation (TT1-[ox]mbELP). M: marker. Protein bands were visualized via TT1 fluorescence under UV light. Uncropped image is shown in Figure S15. (D) Elution profiles of TT1-mbELP before (black) and after (dashed red) light irradiation using the Polaris C8 column. (E) Cryo-TEM imaging of NP1–4. The nanoclusters are shown in white circles. Zoom-in images of NP2 and 4 are further shown in inset (scale bar 25 nm), with the blue arrows pointing to the clusters. The black spots with blurred edges, indicated with white arrows, correspond to ice crystals.

labeled with Cy3, some nanoclusters which were formed with non-labeled dbELP were visualized via only the TT1 signal, resulting in differences in Cy3 and TT1 intensities. The Pearson's coefficients of TT1 and Cy3 from NP4 were 0.35 and 0.66 after 1.5 and 3 hours, respectively, both of which were lower than the ones from NP3. While it is more complicated to compare the coefficients at the later stage (3 hours) due to cellular processes in endosomes, there was a significant difference in the coefficients between NP3 and NP4 at 1.5 hours. This evidence of different Cy3 and TT1 distribution again confirmed disassembly. After 3 hours, the mean fluorescence intensity (FI) from Cy3 and TT1 originating from NP3 was 1.8-fold and 1.5-fold higher, respectively than for NP4 (Figure S8). NP1 and NP2 showed negligible mean FI (Figure S8). Overall data suggested that signals in NP4 was the consequence of targeted delivery and that 7D12-dbELP and TT1-mbELP co-clustered after light irradiation. In line with the cell uptake study, intracellular ROS production, upon photo-irradiation for 15 min, was also observed for NP3 and 4 (Figures 2B and S10) but not for NP1 and NP2 in A431 cells. We also tested NP1–4 using another EGFR-positive MDA-MB-468 cell line,[21] in which a similar uptake phenomenon was observed for NP3 and NP4 (Figure S9).

To see whether the smaller sized nanoclusters would show enhanced tissue penetration, we incubated the above platforms for 3 hours with 250–300 μm spheroids grown from A431 cells as a tumor tissue mimicking in vitro model. Spheroids were then washed with PBS and fixed using paraformaldehyde before embedding them in collagen gels for imaging. To visualize the core of the spheroids, which is limited by the laser penetration depth, a clearance step using a fructose solution was performed.[22] There were limited signals from Cy3 and TT1 from NP1 (Figure 3A), indicating that only few particles had accumulated in the spheroids due

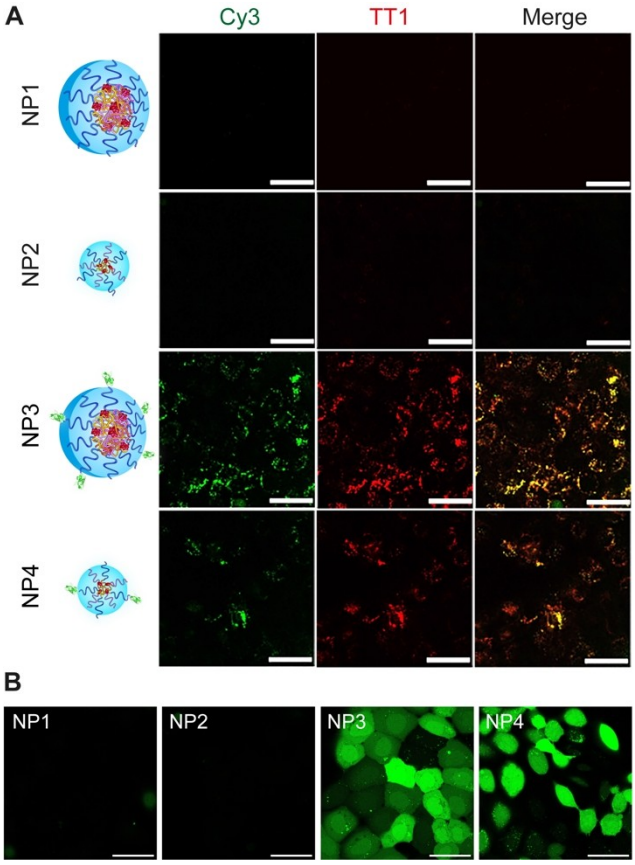

Figure 2. (A) Cell uptake of NP1–4 in A431 cells after 3 hours. DbELP was visualized via Cy3 channel and TT1-mbELP was visualized via TT1 channel. (B) Detection of intracellular reactive oxygen species (ROS) via the DCFH-DA fluorescence probe in A431 cells. ROS was detected after 15 min light irradiation of A431 cells treated with NP3 and NP4 for 3 hours but not seen in ones conducted with NP1 or NP2. Scale bar 50 μm.

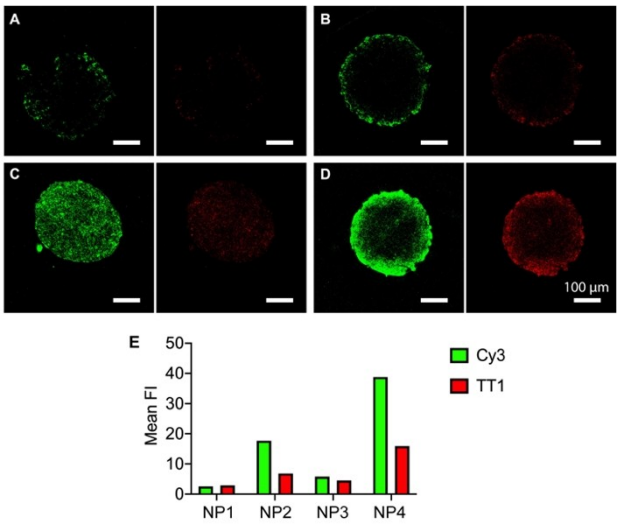

Figure 3. Penetration profiles of ELP NPs into A431 spheroids after 3 hour incubation. (A) NP1, (B) NP3, (C) NP2 and (D) NP4. Cy3 (dbELP) and TT1 (mbELP) channels are depicted in green and red, respectively. (E) Mean fluorescence intensity (FI) of Cy3 and TT1 from NP1–4 in the equatorial planes of the spheroids.

to the lack of a targeting function and the size limitation (>100 nm). By comparison, NP3 showed higher TT1 and Cy3 intensities (Figure 3B), mostly found at the periphery of the spheroid because of size limitations. In contrast, nanoclusters showed greater diffusion into spheroids due to their relatively small sizes. For NP2, signals from Cy3 and TT1 were distributed homogeneously throughout the spheroids (Figure 3C). For NP4, fluorescence showed a gradient from the edge towards the center which can be explained by a binding-site barrier (Figure 3D).[23] It should be noted that the detected signals do not reflect whether NPs were located intra- or extracellularly. Cy3 and TT1 fluorescence intensity distributions along the diameters of spheroids in Figure 3A are shown in Figures S11 and S12. The data indicated that indeed the nanoclusters (NP2 and NP4) had not only enhanced penetration but also higher accumulation, reflected by the higher intensities of both Cy3 and TT1. Mean FI at the equatorial planes of spheroids indicated that NP4 had ≈2-fold higher signals of Cy3 and TT1 compared to NP2, demonstrating the activity of the targeting function (Figure 3E). NP4 also outperformed NP1 and NP3 with ≈9.5-fold higher fluorescence for Cy3 and 4.5-fold higher fluorescence for TT1, respectively (Figure 3E). Overall, these results confirm that small nanoclusters have enhanced penetration compared to intact NPs. While we have utilized 10% of the total ELPs for the targeted ELP, adjusting the percentage of 7D12-dbELP could be further employed in rationally tuning between efficacy for tissue penetration and tissue targeting.

After confirming cellular uptake and tissue penetration, in vitro PDT treatments were conducted in 2D cell layers and 3D spheroids with the expectation that the targeted platforms would outperform non-targeted ones due to the effective delivery of the PS. Before PDT treatment, a dark toxicity assay was performed to confirm that these ELP nanoplatforms did not have cell-killing effects without light irradiation (Figure S13). Furthermore, irradiation using PS-loaded NPs did not result in a temperature increase (Figure S14); therefore, artifacts from thermal effects can be excluded. We first explored PDT efficiency for cells treated with NP1 and NP3. The TT1-mbELP, which forms micro-sized coacervates, was also included as a control. After 1.5 hour incubation, A431 cells were treated for 15 min using a 660 nm laser light source (0.12 $W cm^{-2}$). As shown in Figure 4A, neither the TT1-mbELP conjugate alone nor NP1 showed phototoxicity at 1.0 μM of the PS. By comparison, NP3 loaded with 1.0 μM TT1 were highly efficacious, with >96% cell killing after illumination and 84% cell killing at 0.25 μM TT1. At 0.1 μM TT1 still 30.5% cell-killing was observed (Figure 4A). Noteworthy, the effective doses of TT1 in this study were in a sub-micromolar range even though cells were treated only for a relatively short time (1.5 hours) compared to other reported systems,[24] demonstrating the benefit of active targeting by 7D12. Subsequently, the activities of NP3 and NP4 were compared (Figure 4B). In this 2D tissue culture, there was no significant difference between efficacies of the two platforms

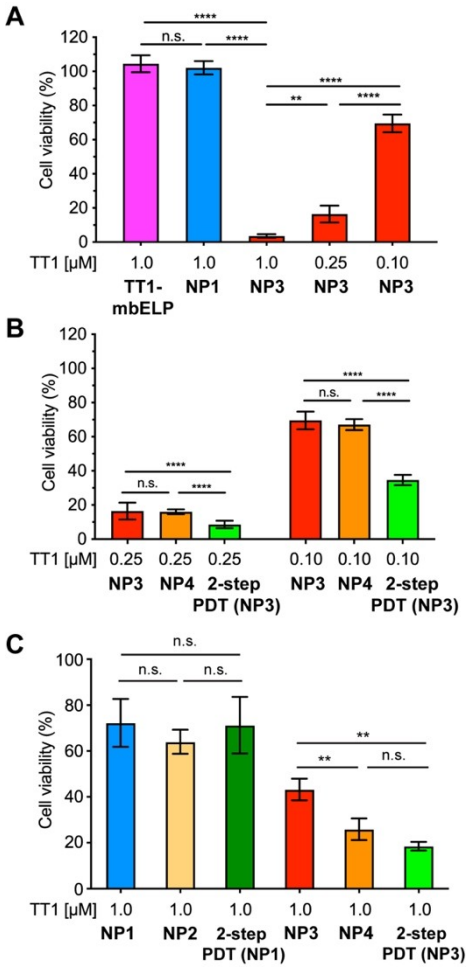

Figure 4. In vitro PDT treatment efficacies studied by cytotoxicity assays in a 2D cell culture (A, B) and in a 3D spheroid (C) model.

at 0.25 μM and 0.10 μM (Figure 4B). In addition, a two-step PDT was also carried out, in which NP3 were first treated by light for 5 min after 30 min incubation to convert them into nanoclusters (NP4). After another 1 hour incubation, a second PDT treatment was carried out for 10 min to induce cell-killing. As shown in Figure 4B, the two-step PDT showed 2-fold enhanced efficiencies (8.6 % and 34.7 % cell viability) in cell killing at 0.25 and 0.10 μM TT1, respectively. This suggested the 2-step PDT was more efficient as the IC_{50} was shifted to a lower dose range. We hypothesize that targeted NPs (NP3) rapidly bound and were taken up within the first 30 min incubation, allowing high accumulation in A431 cells. The first PDT disassembled NP3 into nanoclusters. The second PDT then led to a higher efficacy because of the increased amount of intracellular NP4. Furthermore, the intracellular disassembly could also lead to a better utilization of TT1 and/or oxygen diffusion, due to diminished stacking or encapsulation in the hydrophobic core as in NP3.[25,26]

Finally, the efficacies of NP1–4 were tested using A431 spheroids, given that the targeted nanoclusters (NP4) penetrated deeper into the spheroids. Spheroids were incubated with NPs for 24 hours and then irradiated with a 660 nm laser light (0.12 $W\,cm^{-2}$) for 15 min. As shown in Figure 4C, there was no significant difference between NP1 and NP2. Both killed approximately ≈27 % of cells from the spheroids. NP3 performed better with 57 % cells killed, which can be attributed to the targeting function. NP4 outperformed the other formulations with more than 74 % cell death, which is consistent with the observed higher tissue penetration (Figure 3) and high efficacies in the 2D experiment (Figure 4B). The two-step PDTs using NP1 and NP3 were also carried out to first deliver intact NPs to tumor tissues and then to disassemble them to form nanoclusters for enhanced tissue penetration and PDT. The first 5 min PDT was performed 3 hours post-incubation to convert NP1 and NP3 into NP2 and NP4, respectively. After another 21 hour incubation, spheroids were treated with 10 min irradiation. The two-step process performed with NP1 showed comparable treatment efficacies as their non-targeted counterparts (NP1 and NP2) (Figure 4C), indicating that no improvement in efficacy was achieved, despite enhanced penetration, likely because of the inefficient intracellular PS delivery. In contrast, spheroids that were incubated initially with NP3 which were then converted into NP4 showed lower viability than the other samples (Figure 4C) with 81.5 % cells killed, illustrating the targeted photo-toxicity after disassembly. Importantly, cell killing was as efficient as observed for spheroids directly incubated with NP4.

For future in vivo application, the NPs could be first administered intravenously using the 120 nm targeted NPs (NP3) for longer circulation time and tumor accumulation.[2] In situ light-irradiation would induce transformation into small NP4 to further facilitate tumor penetration as well as targeted delivery for more efficient treatments. A potential hurdle could be that NP3 is affected from shear stress during circulation leading to phase separation of TT1-mbELP and dbELP before reaching the tumor. Given that ELPs can be modularly engineered, the stability however can be fine-tuned by controlling for example the number of Phe residues to enhance hydrophobic interactions.

Conclusion

In summary, this work describes a novel design of size-switchable polymeric NPs that rapidly respond to a NIR-light stimulus (5 min) by partial disassembly and re-organizing, while retaining their targeting function and PDT activity. We demonstrate enhanced tissue penetration and highly effective PDT treatment in 2D and 3D in vitro models. The system is based on the co-assembly of various thermo-responsive ELP modules into homogeneous co-assembled NPs by rapid heating.[18] Generally, ELP NPs are known for their temperature responsiveness. However, for obvious reasons, disassembly of NPs by lowering the temperature cannot easily be applied in vivo. Here we demonstrate that specific disassembly can also be achieved by increasing the T_{cp} in situ by light-induced oxidation of Met-bearing ELPs, giving unique spatiotemporal control. After disassembly, ELP modules, i.e., dbELP and oxidized TT1-mbELP and 7D12-dbELP, likely interact via π-π stacking to form relatively homogeneous small nanoclusters (≈24 nm). Therefore, the newly formed nanostructures still have the targeting function, allowing efficient PS delivery and PDT treatment. Such light-responsive targeted systems have not been reported yet to the best of our knowledge. The systems could also be expanded to co-deliver additional cargos via additional conjugation to TT1-mb, such as chemotherapeutics or immunomodulatory factors for multimodal therapies. We believe that this work will contribute significantly to the design of stimulus-responsive NPs that could be potentially used for tackling some of the hurdles in anticancer treatment.

Acknowledgements

This work was supported by EuroNanoMed3 TEMPEAT and SIRIC Brio Commucan projects. We also thank financial support to MINECO (PID2020-116490GB-I00, Porphyrinoids) and PCIN-2017-042, TEMPEAT), the Comunidad de Madrid (MAD2D-CM) and MICINN through project "Materiales disruptivos bidimensionales (2D)" within the Planes Complementarios (Materiales avanzados). The Nouvelle Aquitaine Region and the FRM are also thanked for financial support. IMDEA Nanociencia acknowledges support from the ''Severo Ochoa'' Programme for Centres of Excellence in R&D (MINECO, Grant SEV-2016-0686).

Conflict of Interest

The authors declare no conflict of interest.

Data Availability Statement

The data that support the findings of this study are available from the corresponding author upon reasonable request.

Keywords: Elastin-Like Peptides · Nanomedicine · Photodynamic Therapy · Self-Assembly · Stimuli-Responsive

[1] M. Izci, C. Maksoudian, B. B. Manshian, S. J. Soenen, *Chem. Rev.* **2021**, *121*, 1746–1803.
[2] J. Wang, W. Mao, L. L. Lock, J. Tang, M. Sui, W. Sun, H. Cui, D. Xu, Y. Shen, *ACS Nano* **2015**, *9*, 7195–7206.
[3] A. Banstola, K. Poudel, J. O. Kim, J. H. Jeong, S. Yook, *J. Controlled Release* **2021**, *337*, 505–520.
[4] Y. R. Zhang, R. Lin, H. J. Li, W. ling He, J. Z. Du, J. Wang, *Wiley Interdiscip. Rev. Nanomed. Nanobiotechnol.* **2019**, *11*, e1519.
[5] K. Deng, C. Li, S. Huang, B. Xing, D. Jin, Q. Zeng, Z. Hou, J. Lin, *Small* **2017**, *13*, 1702299.
[6] Y. Wang, Y. Deng, H. Luo, A. Zhu, H. Ke, H. Yang, H. Chen, *ACS Nano* **2017**, *11*, 12134–12144.
[7] Y. Qin, F. Tong, W. Zhang, Y. Zhou, S. He, R. Xie, T. Lei, Y. Wang, S. Peng, Z. Li, J. Leong, H. Gao, L. Lu, *Adv. Funct. Mater.* **2021**, *31*, 2104645.
[8] J. Pille, S. A. M. van Lith, J. C. M. van Hest, W. P. J. Leenders, *Biomacromolecules* **2017**, *18*, 1302–1310.
[9] S. A. M. van Lith, D. van den Brand, R. Wallbrecher, L. Wübbeke, S. M. J. van Duijnhoven, P. I. Mäkinen, J. S. Hoogstad-van Evert, L. Massuger, S. Ylä-Herttuala, R. Brock, W. P. J. Leenders, *Eur. J. Pharm. Biopharm.* **2018**, *124*, 63–72.
[10] D. H. T. Le, A. Sugawara-Narutaki, *Mol. Syst. Des. Eng.* **2019**, *4*, 545–565.
[11] N. K. Li, F. G. Quiroz, C. K. Hall, A. Chilkoti, Y. G. Yingling, *Biomacromolecules* **2014**, *15*, 3522–3530.
[12] J. R. McDaniel, D. C. Radford, A. Chilkoti, *Biomacromolecules* **2013**, *14*, 2866.
[13] M. Abdelghani, J. Shao, D. H. T. Le, H. Wu, J. C. M. van Hest, *Macromol. Biosci.* **2021**, *21*, 2100081.
[14] V. Ibrahimova, J. A. González-Delgado, M. Levêque, T. Torres, E. Garanger, S. Lecommandoux, *Bioconjugate Chem.* **2021**, *32*, 1719–1728.
[15] M. García-Iglesias, J. J. Cid, J. H. Yum, A. Forneli, P. Vázquez, M. K. Nazeeruddin, E. Palomares, M. Grätzel, T. Torres, *Energy Environ. Sci.* **2011**, *4*, 189–194.
[16] G. Martínez-Edo, E. Y. Xue, S. Y. Y. Ha, I. Pontón, J. A. González-Delgado, S. Borrós, T. Torres, D. K. P. Ng, D. Sánchez-García, *Chem. Eur. J.* **2021**, *27*, 14610–14618.
[17] R. Petitdemange, E. Garanger, L. Bataille, W. Dieryck, K. Bathany, B. Garbay, T. J. Deming, S. Lecommandoux, *Biomacromolecules* **2017**, *18*, 544–550.
[18] J. Pille, A. Aloi, D. H. T. Le, I. Vialshin, N. van de Laar, K. Kevenaar, M. Merkx, I. K. Voets, J. C. M. van Hest, *Small* **2021**, *17*, 2007234.
[19] H. Hong, Z. Zhou, K. Zhou, S. Liu, Z. Guo, Z. Wu, *Chem. Sci.* **2019**, *10*, 9331–9338.
[20] F. Zhang, S. Wang, L. Yin, Y. Yang, Y. Guan, W. Wang, H. Xu, N. Tao, *Anal. Chem.* **2015**, *87*, 9960–9965.
[21] A. El Guerrab, M. Bamdad, F. Kwiatkowski, Y. Bignon, F. Penault-Llorca, C. Aubel, *Oncotarget* **2016**, *7*, 73618–73637.
[22] L. M. P. E. van Oppen, J. Pille, C. Stuut, M. van Stevendaal, L. N. van der Vorm, J. A. M. Smeitink, W. J. H. Koopman, P. H. G. M. Willems, J. C. M. van Hest, R. Brock, *Eur. J. Pharm. Biopharm.* **2019**, *137*, 175–184.
[23] K. Fujimori, D. G. Covell, J. E. Fletcher, J. N. Weinstein, *J. Nucl. Med.* **1990**, *31*, 1191–1198.
[24] M. Czarnecka-Czapczyńska, D. Aebisher, P. Oleś, B. Sosna, M. Krupka-Olek, K. Dynarowicz, W. Latos, G. Cieślar, A. Kawczyk-Krupka, *Biomed. Pharmacother.* **2021**, *144*, 112342.
[25] X. Li, M. Ke, M. Zhang, Q. Tang, B. Zheng, J. Huang, *Chem. Commun.* **2015**, *51*, 4704–4707.
[26] B. Ghazal, A. Husain, A. Ganesan, M. Durmuş, X. Zhang, S. Makhseed, *Dyes Pigm.* **2019**, *164*, 296–304.

Manuscript received: January 11, 2023
Accepted manuscript online: April 21, 2023
Version of record online: ■■, ■■

Research Articles

Nanoparticles

D. H. T. Le, V. Ibrahimova,
S. A. H. van den Wildenberg, H. Wu,
A. Fonseca, T. Torres, E. Garanger,
W. P. J. Leenders, R. Brock,
S. Lecommandoux,
J. C. M. van Hest* _____ **e202300511**

Light-Responsive Elastin-Like Peptide-Based Targeted Nanoparticles for Enhanced Spheroid Penetration

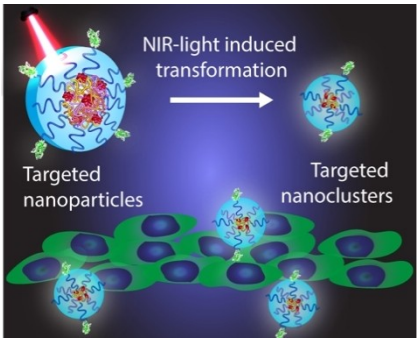

A near infrared (NIR)-light-responsive targeted nanoparticle based on elastin-like polypeptides and loaded with photosensitizers, is able to transform rapidly into a small nanocluster for enhanced penetration into spheroids. The nanocluster still has its targeting function and thus is highly efficient in both cargo delivery and cell-killing in photodynamic therapy.

Supporting Information

Light-Responsive Targeted Elastin-Like Peptide-Based Nanoparticles for Enhanced Spheroid Penetration

Duc H. T. Le, Vusala Ibrahimova, Sebastian A. H. van den Wildenberg, Hanglong Wu, Alba Fonseca, Tomas Torres, Elisabeth Garanger, William P. J. Leenders, Roland Brock, Sébastien Lecommandoux, Jan C. M. van Hest*

Abstract: We describe here a near infrared light-responsive elastin-like peptide (ELP)-based targeted nanoparticle (NP) that can rapidly switch its size from 120 to 25 nm upon photo-irradiation. Interestingly, the targeting function, which is crucial for effective cargo delivery, is preserved after transformation. The NPs are assembled from (targeted) diblock ELP micelles encapsulating photosensitizer TT1-monoblock ELP conjugates. Methionine residues in this monoblock are photo-oxidized by singlet oxygen generated from TT1, turning the ELPs hydrophilic and thus trigger NP dissociation. Phenylalanine residues from the diblocks then interact with TT1 *via* π-π stacking, inducing the re-formation of smaller NPs. Due to their small size and targeting function, the NPs penetrate deeper in spheroids and kill cancer cells more efficiently compared to the larger ones. This work could contribute to the design of "smart" nanomedicines with deeper penetration capacity for effective anticancer therapies.

DOI: 10.1002/anie.202300511

Table of Contents

Materials and Methods

Preparation of ELP-encoding plasmids

Pairs of single stranded DNAs that encode the sense and the antisense strands of the basic repeating motifs in ELPs were purchased from EU Integrated DNA Technologies (EU IDT). A pair of oligonucleotides in a T4 ligase buffer was annealed at 95ºC for 2 min and then gradually cooled down to room temperature to obtain the genes encoding the basic repeating motifs in the hydrophilic and hydrophobic block, i.e. [A_3G_2] and [V_4F_1]. Concatemerization of these units was carried out and the ELP open reading frames (ORF) were cloned in pET24a(+). ELP blocks [A_3G_2-60] and [V_4F_1-50], were selected and combined using recursive directional ligation to obtain pET24a(+)-[A_3G_2-60]-[V_4F_1-50].[1] For the targeting dbELP, a gBLOCK containing the ORF of the targeting nanobody 7D12, preceded by the pelB signal sequence was ordered from EU IDT. The fragment was introduced into the pET24a(+)-[A_3G_2-60]-[V_4F_1-50] vector via *XbaI* and *AcuI* double digestion. All plasmids were confirmed by Sanger sequencing. The plasmid pET44a(+)-[M_1V_3-40] encoding the mbELP was previously generated by Ibrahimova *et al*.[2]

Protein expression and purification

The plasmids were transformed into *E. coli* BL21(DE3) (Thermo Fisher) for expression. A single colony from each construct was picked and grown in LB cultures containing 50 µg/mL kanamycin (Sigma-Aldrich) and 0.5% (w/v) D-glucose (Sigma-Aldrich). Once the OD600 reached 0.8, small cultures were transferred into filter-sterilized auto induction TB media (Formedium) containing 0.005% Antifoam 204 (Sigma-Aldrich), 6 g/L glycerol (Fisher Chemical) and 150 µg/mL kanamycin. Cultures were kept at 37 ºC for 4 hours and then at 30 ºC for another 20 hours, under shaking at 250 rpm. Cells were pelleted by centrifugation at 8,000 x *g*, 4 ºC, for 20 min.

For cytoplasmic extraction of dbELP, 1 g of wet cell pellet was resuspended in 5 mL Bug Buster Protein Extraction Reagent (Millipore) and incubated for at least 30 min to lyse cells. Cell debris was removed by centrifugation at 15,000 x *g*, 4 ºC for 30 min. Supernatants containing ELPs were collected and further purified by Inverse Transition Cycling (ITC) as previously described.[3] Briefly, ELPs were precipitated by saturated ammonium sulfate (Sigma-Aldrich) and pelleted by centrifugation at 15,000 x *g*, 25 ºC for 30 min. ELP pellets were then re-suspended in cold PBS supplemented with cOmplete protease inhibitor cocktails (Roche), while insoluble fractions were separated by centrifugation at 15,000 x *g*, 4 ºC for 30 min. The cycle was repeated 3-4 rounds before applying the purified product to a HiLoad 16/600 Superdex 200 column (GE Healthcare Life Sciences) on a Bio-Rad NGC chromatography system with a flow rate of 1 mL/min MilliQ water. The product purity was verified by SDS-PAGE (Figure S1) and the molecular weights were determined using Quadrupole Time of Flight Q-ToF LC/MS mass spectrometry (Table S1). Samples were stored in lyophilized powder form prior to use. The yields of dbELP and mbELP were typically ranging from 80–100 mg per L culture.

Periplasmic extraction of 7D12-[A_3G_2-60]-[V_4F_1-50] was carried out as described by Pille *et al*.[3] Briefly, the cell pellet was resuspended in extraction buffer A containing 0.2 M Tris (Sigma-Aldrich) pH 8.0, 0.5 mM EDTA (Sigma-Aldrich), 20% w/v sucrose (Sigma-Aldrich) and protease inhibitor cocktails. The suspension was incubated for 30 min at 4 ºC, followed by centrifugation (5,000 x *g*, 4 ºC, 30 min). The supernatant containing 7D12-dbELPs was collected and the pellet was resuspended in extraction buffer B (0.2 M Tris pH 8.0, 15 mM $MgSO_4$) and protease inhibitor cocktails. After centrifugation (5,000 x *g*, 4 ºC, 30 min) the supernatant was pooled with the first supernatant. The targeted dbELP was then purified by ITC and size exclusion chromatography. SDS-PAGE and Q-Tof LC/MS were conducted for confirmation of purity and determination of the molecular weight, respectively (Figure S1 and Table S1). A typical yield of 7D12-dbELP was approximately 25 mg per L culture.

Synthesis of TT1-[M_1V_3-40] conjugate

TT1-amide C3 azide was prepared and conjugated to [M_1V_3-40] according to Ibrahimova *et al*.[2] Briefly, the N-terminal amine from [M_1V_3-40] was converted into an alkyne handle via an NHS-amine coupling reaction using 4-pentynoic acid succinimidyl ester. After purification to remove unreacted reagents, TT1-amide C3 azide was added for orthogonal bioconjugation. The products were purified via the ITC method.[2,3] The molecular weights of the final products were confirmed by Q-ToF LC/MS (Table S1). The final yield after reaction and ITC purification was 23%.

Determining the cloud point temperature (T_{cp}) of the dbELP

DbELP was dissolved in PBS to a final concentration of 10 µM. The solution was gradually heated from 15 to 60 ºC with a ramping rate 0.1 ºC/min. Dynamic Light Scattering (DLS) was used to record the changes in hydrodynamic diameter of the nanostructures with increasing temperatures.

Formation of co-assembled nanoparticles (NPs)

Both the dbELP [A_3G_2-60]-[V_4F_1-50] and the TT1-mbELP conjugate were dissolved in dry dimethyl sulfoxide (DMSO) (Thermo Fisher) to a final concentration of 1 mM as stock solutions. The dbELP and the mbELP conjugate were mixed at a 1:1 molar ratio. The co-assembly was induced by directly adding pre-heated PBS or cell culture medium into the dbELP-mbELP mixture, followed by three-time pipetting. For targeting NPs, 7D12-[A_3G_2-60]-[V_4F_1-50] in PBS was also included so that the final molar ratio became 1:4:5 for 7D12-dbELP: dbELP: TT1-mbELP, respectively. Throughout the experiments, the co-assembled NP solutions were maintained at 37 ºC to avoid temperature effects on the self-assembled structures. The final concentration of DMSO was limited to less than 0.5 % (v/v), the concentration at which we did not observe cellular toxicity *in vitro* (data not shown). For lower concentrations, NP suspensions were further diluted in PBS or culture medium (pre-heated at 37 ºC).

Photo-oxidation of co-assembled NPs

Solutions with co-assembled ELP NP were kept in LightSafe microtubes (Sigma-Aldrich) to avoid light exposure and at 37 ºC in a heating block during experiments. To perform photo-oxidation, the NP suspensions were irradiated with a 660-nm laser at 0.12 W/cm^2 for 5 min. Subsequently, photo-irradiated ELP suspensions were subjected to dynamic light scattering (DLS) measurements for size determination. The mass shift in TT1-mbELP before and after photo-irradiation was confirmed by Q-ToF LC/MS and gel electrophoresis SDS-PAGE.

Dynamic Light Scattering (DLS)

NPs were prepared at a 10.0 µM final concentration of total ELPs in PBS buffer. Measurements were performed on a Malvern Zetasizer Nano. Samples were equilibrated at 37 ºC for 5 min before data collection.

Quadrupole Time of Flight (Q-ToF) LC/MS Mass Spectrometry

Masses were determined using a high-resolution LC/MS system consisting of a Waters ACQUITY UPLC I-Class system coupled to a Xevo G2 Quadrupole Time of Flight (Q-ToF). Freeze dried samples were resuspended in MilliQ to a concentration of 1.0 µM. The samples were acidified with 0.1% formic acid upon injection. The protein was separated (0.3 mL/min) on a column (Polaris C8 or C18 reverse phase column 2.0 × 100 mm, Agilent) using a 15–75% (v/v) acetonitrile (Sigma-Aldrich) gradient in water supplemented with 0.1% (v/v) formic acid (Sigma-Aldrich) before analysis in positive mode in the mass spectrometer. Deconvolution of the m/z spectra was performed using the MaxENTI algorithm in the Masslynx v4.1 (SCN862).

Cryogenic Transmission Electron Microscopy (cryo-TEM)

The morphologies of the ELP NPs, before and after light irradiation, were characterized on a CryoTitan (ThermoFisher Scientific) equipped with a field-emission gun operating at 300 kV, a post-column Gatan energy filter and an autoloader station. The grids (R2/2, Cu, Quantifoil Jena grids, Quantifoil Micro Tools GmbH) for cryo-TEM imaging were first treated in a Cressington 208 carbon coater for 40 s. Then, 3 µL of sample solution was pipetted onto the grid and blotted in a Vitrobot MARK IV (ThermoFisher Scientific) at 37 °C with 100% humidity. The grid was blotted for 3.5 s (blotting force -1) and directly plunged and frozen in liquid ethane. Images were acquired using a post-GIF 2k GATAN CCD (charged-coupled device) camera.

UV-Vis Spectroscopy

Absorbances of TT1 encapsulated in the co-assembled ELP NPs and in the nanoclusters after photo-irradiation were monitored by an Agilent Cary 100 UV−vis spectrophotometer. Temperature was set at 37 ºC during measurement.

Temperature changes during photo-irradiation

ELP NP1–4 loading 1 µM TT1 as well as PBS, as a control, were kept at 37 ºC during photo-irradiation. Solutions were photo-irradiated by a 660-nm laser light (0.12 W/cm^2) for 15 min. Solution temperatures were measured and recorded by a C.A 1821 thermo-couple thermometer (Chauvin Arnoux).

Conjugation of dbELP with sulfo-Cy3 and preparation of fluorescently labeled NPs

DbELP was dissolved in DMSO to a final concentration of 500 µM. To this solution, amino-reactive sulfo-Cyanine3 NHS ester (Lumiprobe) was added at a molar ratio 1.5 sulfo-Cy3:1 dbELP to label the *N*-terminal amine group. The reaction was allowed to proceed at room temperature for 24h. Cy3-dbELP was purified using a PD MidiTrap G-25 column (GE Healthcare) and dialyzed towards MilliQ water. The product was freeze-dried to obtain the lyophilized powder for storage at -20 ºC prior to use.

To prepare fluorescently labeled NPs for confocal microscopic studies, Cy3-dbELP, dbELP, and TT1-mbELP were mixed in the molar ratio of 1:4:5 and the co-assembly method was used to induce NP formation. Similarly, targeting NPs were prepared using 7D12-dbELP, Cy3-dbELP, dbELP, TT1-mbELP in the molar ratio of 1:1:3:5.

Cell culture

Human epidermoid carcinoma A431 and human breast adenocarcinoma MDA-MB-468 cells overexpressing the epidermal growth factor (EGF) receptor were cultured in DMEM (Lonza, Basel, Switzerland) supplemented with 10% FCS (Gibco) and 40 µg/mL Glutamax (Thermo Fisher Scientific). Cells were cultured at 37 °C in 5% CO_2 in a humidified atmosphere.

Cellular uptake of various ELP NP platforms

A431 cells were seeded and grown in RPMI 1640 medium (Thermo Fisher Scientific), supplemented with 10% FCS and 1% Glutamax, in an 8-well chambered coverslip (Ibidi). Cell cultures were maintained at 37 ºC in a humidified atmosphere containing 5% CO_2. Cells were washed with PBS and exchanged with fresh media containing various platforms of ELP NPs with the final concentration of 2.0 µM (1.0 µM TT1). After 1.5- or 3-hour incubation, cells were washed once with PBS to remove unbound ELPs and replaced with fresh RPMI medium. Cells were subsequently imaged using a Leica 63x/1.2 water immersion objective lens from an SP8 confocal microscope (Leica Microsystems, Manheim, Germany). NPs were detected via both the photosensitizer TT1 attached to the mbELP and Cy3 attached to the dbELP. A white light laser was used to excite Cy3 at 550 nm and TT1 at 640 nm. Emission was collected between 580 and 600 nm for Cy3 and between 650 and 700 nm for TT1. Images were processed using FIJI (http://fiji.sc/). The same brightness and contrast settings were applied for all images at the same experimental conditions. A similar procedure for the cell uptake study using MDA-MB-468 was also performed.

Quantification of intracellular mean fluorescence intensity

Fluorescence intensity was measured using FIJI (http://fiji.sc/). First, the same settings of the color thresholds were adapted for the four NP1–4 platforms. Five random cells in an image were selected and regions of interests (ROIs) were defined to determine the raw mean fluorescence intensity per cell. These were subtracted from the mean background signal selected outside the cells. Data were shown as average ± standard deviation (n = 5). Statistical comparisons were made using one-way ANOVA performed in GraphPad Prism ver 9.0. Significant difference was defined at P values < 0.05.

Colocalization test

Colocalization of intracellular Cy3 and TT1 signals was determined via Just Another Colocalization Plugin (JACoP) in FIJI (http://fiji.sc/) to obtain Pearson's coefficients.[5] The same color threshold was adapted for all images before analyzing.

Detection of intracellular reactive oxygen species (ROS)

A ROS assay kit containing highly sensitive and cell-permeable DCFH-DA (2',7'-dichlorodihydrofluorescein diacetate) was purchased from Dojindo. DCFH-DA, in the present of intracellular ROS, is converted into highly fluorescent DCF (Ex/Em 488/550 nm).

ELP NPs loading 1 µM TT1 were prepared and incubated with A431 cells for 3 hours using the same procedure in the cell uptake study. After washing by PBS, working solutions containing DCFH-DA were added and incubated for 30 min at 37 ºC for cell uptake. Light irradiation was performed for 15 min to generate ROS using the 660-nm laser light source (0.12 W/cm^2). After washing by PBS and replenishing with fresh DMEM medium, intracellular fluorescence was detected using a SP8 confocal microscope.

Cytotoxicity assays

A431 cells were seeded at 5000 cells/well in a 96-well plate and incubated overnight. Cells were washed once with PBS, followed by incubation with RPMI 1640 medium containing non-targeting ELP NPs (NP1) and targeting ELP NPs (NP3) and the corresponding light-induced nanoclusters (NP2 and NP4, respectively). TT1-mbELP at the same TT1 concentration was used as a control. After 1.5 hours of incubation, cells were irradiated with a 660-nm laser light (0.12 W/cm^2) for 15 min. To determine cell viability, CCK-8 reagents (Dojindo) were added into the medium and incubated for 2 hours. Relative cell viability was calculated by the ratio of alive cells in PDT-treated samples vs. alive cells from samples without treatment in the same plate. Cell viabilities from samples incubated with ELP NPs but without photo-irradiation were also determined to investigate dark toxicity.

In a 2-step PDT treatment, cells were first incubated with intact targeting NPs (NP3) for 30 min. The first PDT was carried out for 5 min using a 660-nm laser light (0.12 W/cm^2) to disassemble the NPs extra- and intracellularly. Cells were further incubated for another hour before conducting the second PDT treatment for 10 min. Cell viability was determined using CCK-8 reagents.

Data were calculated in GraphPad Prism ver. 9.0 and were shown as average ± standard deviation with n = 4. Statistical comparisons were made using one-way ANOVA performed in GraphPad Prism ver 9.0. Significant difference was defined at P values < 0.05.

Formation of spheroids and tissue penetration of ELP NPs

A 96-well plate for preparing spheroids was coated with 0.75% (w/v) agarose gels in each well. Suspensions (1 x 10^4 cells per 100 µL per well) of A431 cells were added and cultured on the prepared agarose gel. A single spheroid, with an average diameter of 250 µm, was obtained in each well due to aggregation of A431 cells after three days. The spheroids were washed twice using PBS and incubated later with fresh RPMI 1640 medium containing the ELP NPs. Similarly, ELP NPs were detected via Cy3, attached on the dbELP, and TT1, attached on the mbELP. Three-hour post-incubation, clearance of spheroids was carried out at 37 ºC for confocal imaging as previously published.[4] First, spheroids were washed with pre-heated PBS (37 ºC) and fixed in paraformaldehyde (Sigma) (4% (v/v) in PBS) for 30 min at 37 ºC. Subsequently, fixed spheroids were embedded in collagen (Themo Fisher Scientific) gels in each well from an ibidi chamber. The spheroids were then cleared by incubating in fructose (Sigma-Aldrich) solutions containing 0.5% (v/v) 1-thiolglycerol (Sigma-Aldrich) with increasing fructose concentrations, i.e., 28.75%, 57.5%, and 115% (w/v) at 37 ºC. Spheroids were imaged using the SP8 confocal microscope. Images were processed using FIJI (http://fiji.sc/).

Fluorescence intensity distribution along a diameter of the equatorial plane of a spheroid was analyzed by the Color Profiler Plug-in in FIJI (https://imagej.nih.gov/ij/plugins/color-profiler.html).

The total fluorescence intensity within the equatorial planes of spheroids was analyzed by FIJI. When comparing mean fluorescence intensities of Cy3 or TT1, the same settings of color thresholds were adapted for the four spheroids treated with four NP platforms. A circle was drawn around the edge of a spheroid to define the regions of interest (ROI) so that the raw mean fluorescence intensity per pixel in a spheroid could be calculated. From these, the mean background signal selected outside the spheroids was subtracted.

Cytotoxicity assay in spheroid models

Spheroids were prepared in a 96-well plate as aforementioned. Spheroids were washed and then incubated with fresh media containing ELP NP1–4 (1.0 µM TT1) for 24 hours followed by irradiation (660 nm, 0.12 W/cm^2, 15 min). To determine cell viability, the ViaLight™ Plus Cell Proliferation and Cytotoxicity BioAssay Kit (LONZA) was used. Spheroids were completely lysed using the kit lysis buffer to release intracellular adenosine triphosphate (ATP) from alive cells. Reagents for ATP assays comprising of the substrates and luciferase were added to the cell lysate solution and the bioluminescence was determined. Relative cell viability was calculated by the ratio of alive cells in PDT-treated spheroids vs. alive cells from spheroids without treatments in the same plate. For 2-step PDT, the spheroids were first incubated with intact NP1 or NP3 for 3 hours followed by the first PDT treatment for disassembly of NPs into NP2 and NP4, respectively. Incubation continued for another 21 hours before the second PDT (10 min). Data is shown as the average ± standard deviation from three spheroids treated in the same condition (n = 3). Statistical comparisons were made using one-way ANOVA performed in GraphPad Prism ver 9.0. Values are considered significantly different when p values < 0.05.

Supporting Figures and Tables

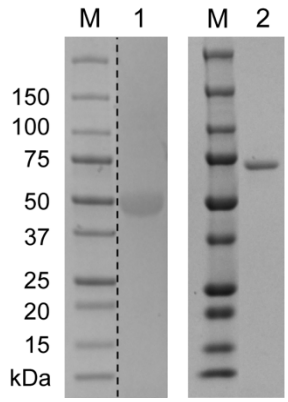

Figure S1. Confirmation of purity of ELPs by gel electrophoresis (SDS-PAGE). (A) dbELP (lane 1) and 7D12-dbELP (lane 2). M: Precision Plus Protein All Blue Prestained Protein Standards. Marker lane (M) and lane 1 were cropped from the original gel shown in Figure S16. Lane separation is indicated by a dashed line.

Table S1. Summary of the protein masses determined by LC-MS/Q-ToF vs. their theoretical masses.

	dbELP	7D12-dbELP	mbELP	TT1-mbELP
Theoretical mass (Da)	43742	58441	17035	17989
Deconvoluted mass (Da)	43742	58421	17035	17988

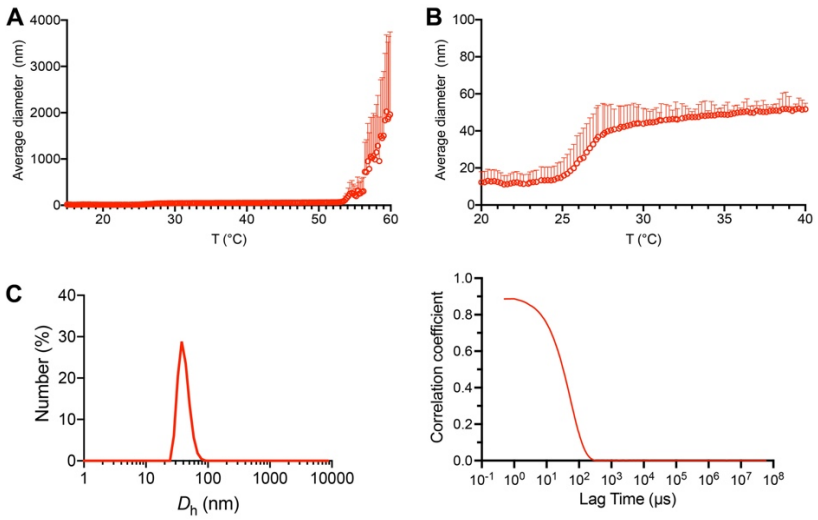

Figure S2. (A,B) Temperature-dependent average hydrodynamic diameters of nanostructures assembled from dbELP [A_3G_2-60]-[V_4F_1-50] determined by DLS. (B) A portion from (A) indicating micelle formation at temperatures higher than 28 ºC. The sizes of micelles ranged from 40-50 nm in diameter. At a temperature higher than 53 ºC, aggregation of dbELP was observed. Data are shown as mean average **+** standard deviation (n = 3). (C) DLS profile (left) and the corresponding correlogram (right) from dbELP based micelles at 37 ºC. The number-derived hydrodynamic diameter of the ELP micelle was 44.9 ± 15.4 nm (PdI 0.01).

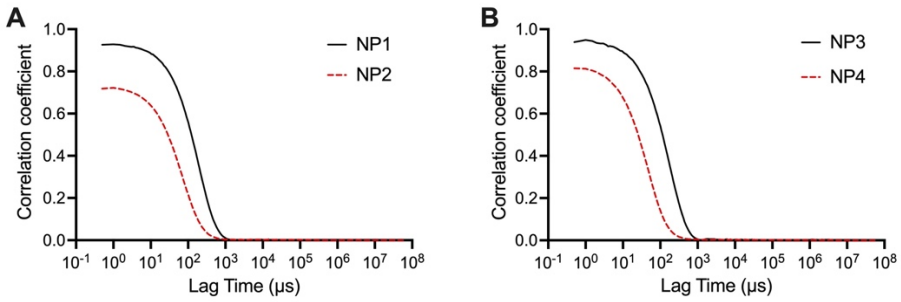

Figure S3. Corresponding correlograms from the DLS profiles of NP1–4 in Figures 1A and 1B. (A) NP1 and NP2. (B) NP3 and NP4.

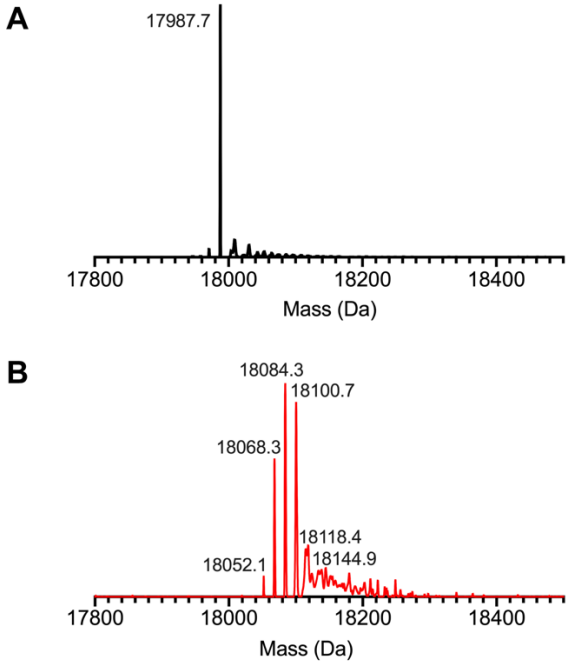

Figure S4. Deconvoluted masses of encapsulated TT1-mbELP in the co-assembled NP in case of (A) without and (B) with light irradiation. The spectra were obtained by deconvoluting the elution peaks of the spectra shown in Figure 2B.

Table S2. Summary of detected masses from Q-ToF LC/MS (Figure S3). One oxidized Met residue will result in an increase of the mass by one oxygen (16 Da). Approximately 5–7 residues were oxidized upon 5-min light irradiation (Figure S3A).

	Without light irradiation	With light irradiation (5 min)					
Detected mass (Da)	17988	18052	18068	18084	18101	18114	18145
Mass increase (Da)		64	80	96	113	130	161
Number of oxidized Met residues		4	5	6	7	8	10

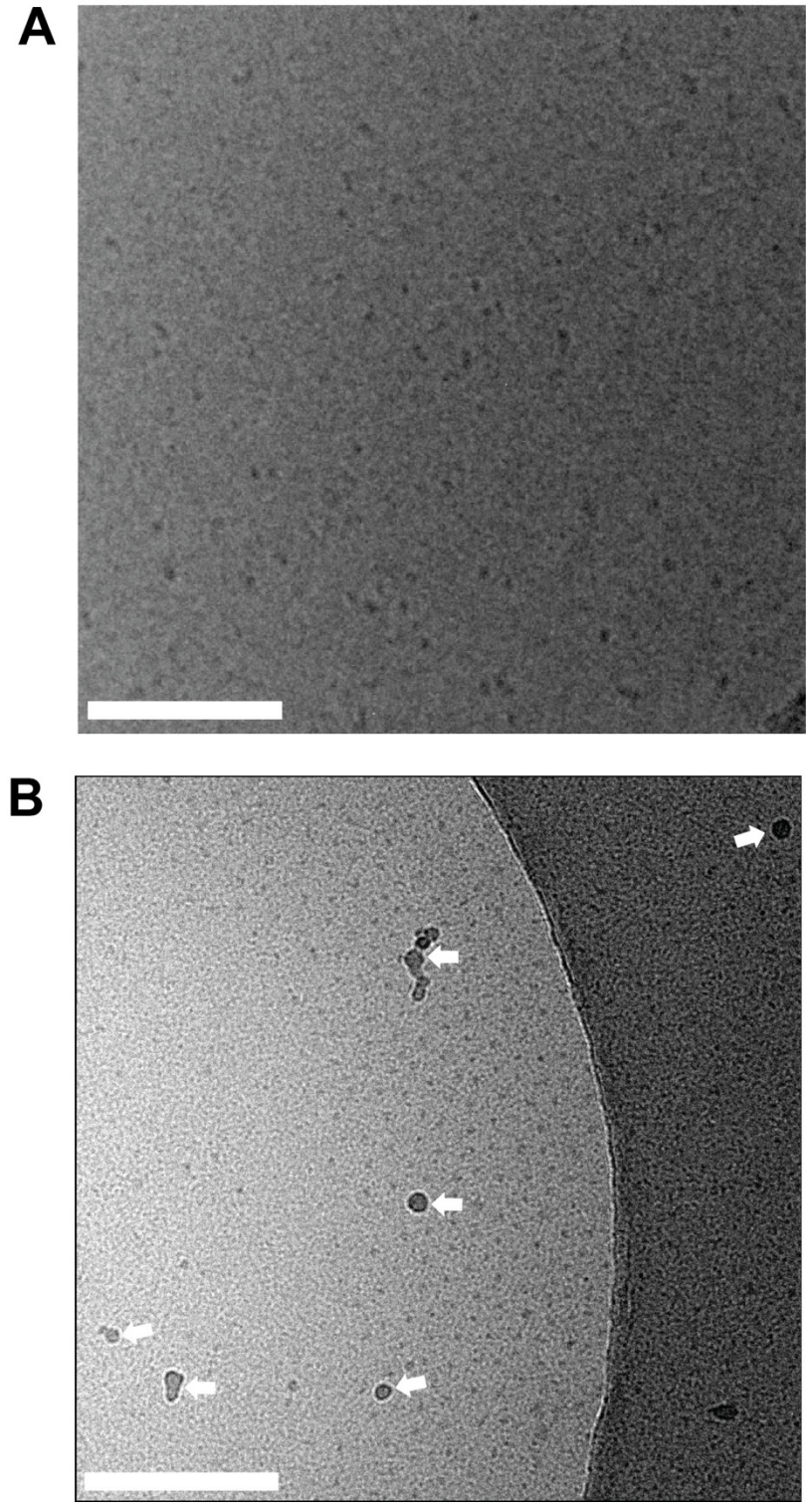

Figure S5. Cryo-TEM imaging of NP2 and NP4 showing formation of nanoclusters. The black spots with blurred edges, indicated with white arrows, correspond to ice crystals. Scale bar 200 nm.

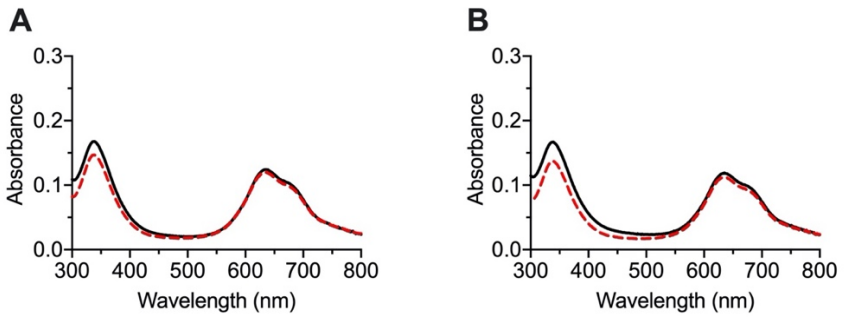

Figure S6. UV-Vis spectroscopy of co-assembled NPs before (black line) and after light irradiation (red dotted line). (A) Non-targeting NPs and (B) targeting NP.

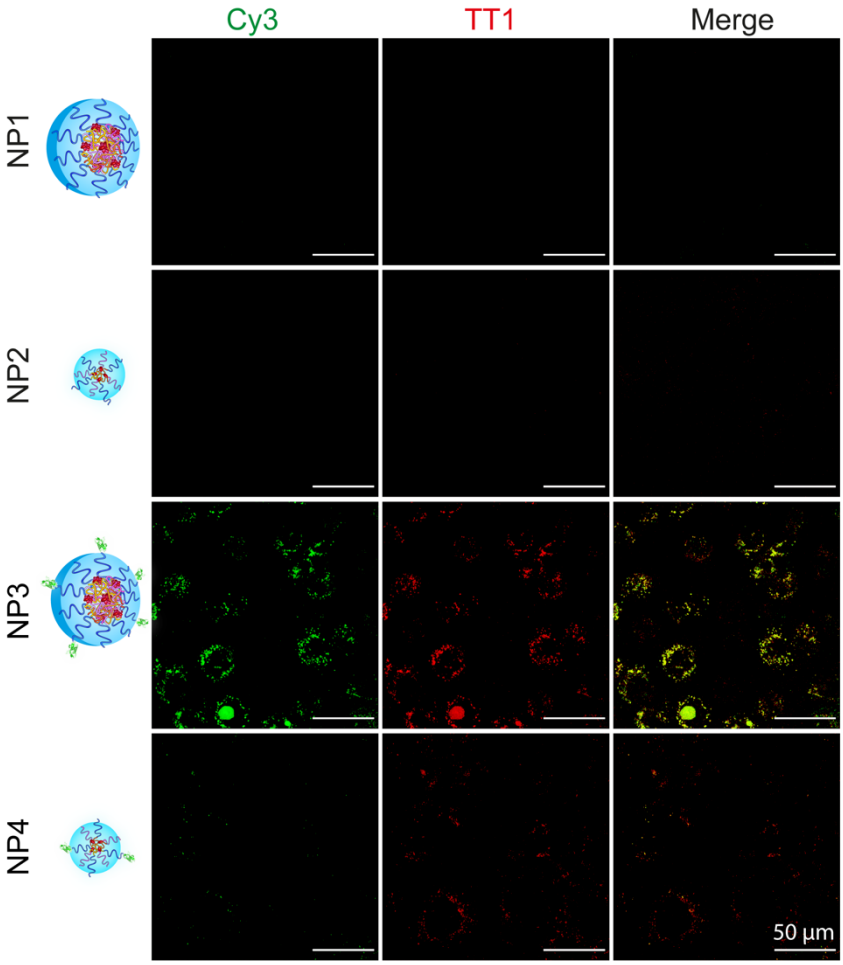

Figure S7. Cell uptake of various NP platforms after 1.5-hour incubation with A431 cells. NPs were visualized via both Cy3, which was conjugated to the N-terminus of the dbELP, and TT1, which was conjugated to the N-terminus of mbELP. Uptake was confirmed for the targeting platforms, i.e., NP3 and NP4 although the Cy3 and TT1 signals were less intense in case of the NP4 compared to NP3 after 1.5 hours. The Pearson's correlation coefficients from NP3 and NP4 were 0.804 and 0.347, respectively. This suggested that at the early stage of the endocytosis, NP3 was likely taken up as intact NPs composed of all ELP components while NP4, due to disassembly, has a lower overlapping degree between Cy3 and TT1.

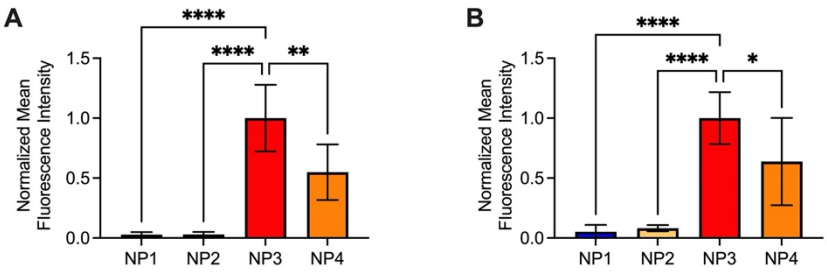

Figure S8. Mean fluorescence intensity (FI) per cell of (A) Cy3 and (B) TT1. A431 cells were incubated with NP1–4 for 3 hours and imaged live using confocal microscopy. After 3-hour incubation, the mean fluorescence intensity (FI) of Cy3 in cells incubated with NP3 was 1.8-fold higher than cells incubated with NP4. Similarly, the mean fluorescence intensity (FI) of TT1 from NP3 was 1.6-fold higher.

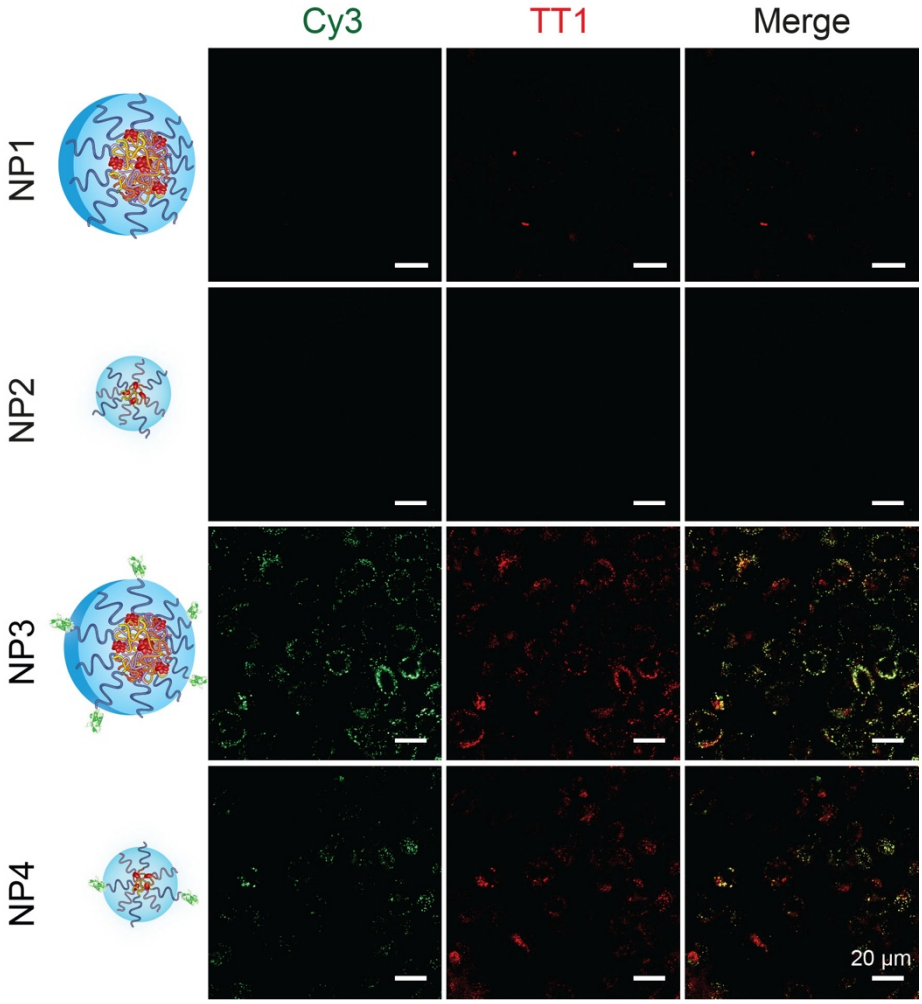

Figure S9. Cell uptake of various NP platforms after 3-hour incubation with a triple negative breast cancer cell line MDA-MB-468, which also expresses high level of EGFR. NPs were visualized via both Cy3, which was conjugated to the N-terminus of the dbELP, and TT1, which was conjugated to the N-terminus of mbELP. Uptake was confirmed for the targeting platforms, i.e., NP3 and NP4, implying the targeting function can be used for other EGFR-positive cell lines. The Pearson's coefficients of NP3 and NP4 were 0.705 and 0.576, respectively, which is consistent with what has been observed in A431 cells.

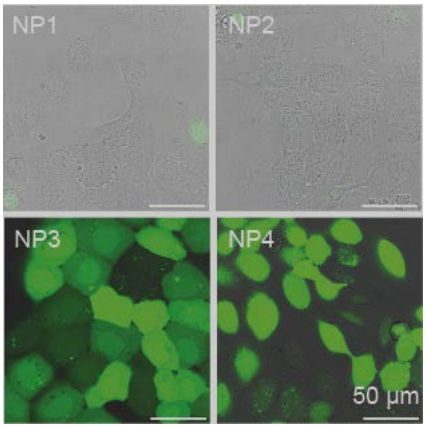

Figure S10. Merged images of the DCFH-DA channel (Ex/Em 480/550 nm) and the bright field channel of A431 cells shown in Figure 2B.

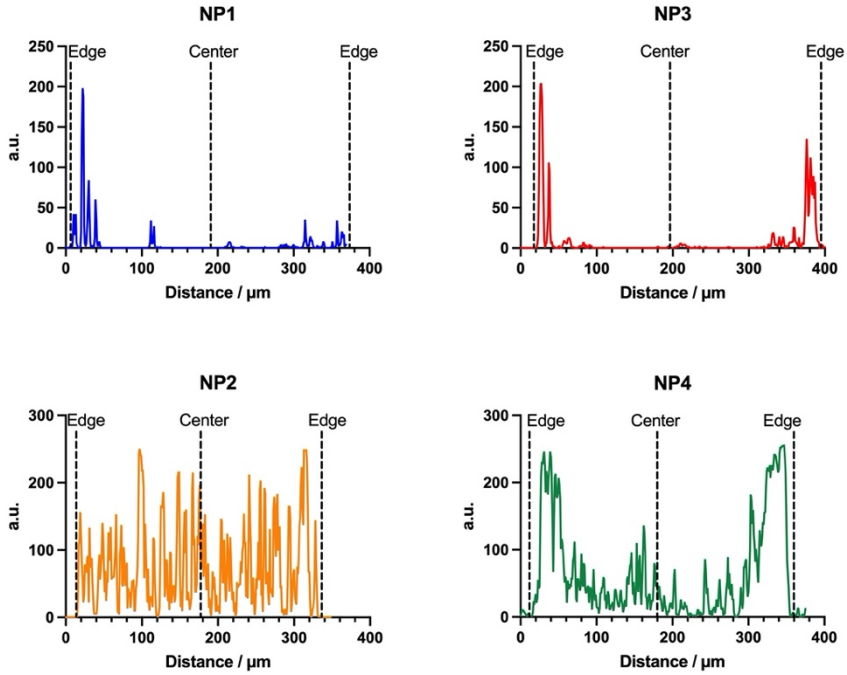

Figure S11. Cy3 fluorescence intensity profiles passing through the equatorial plane section shown in Figure 3A.

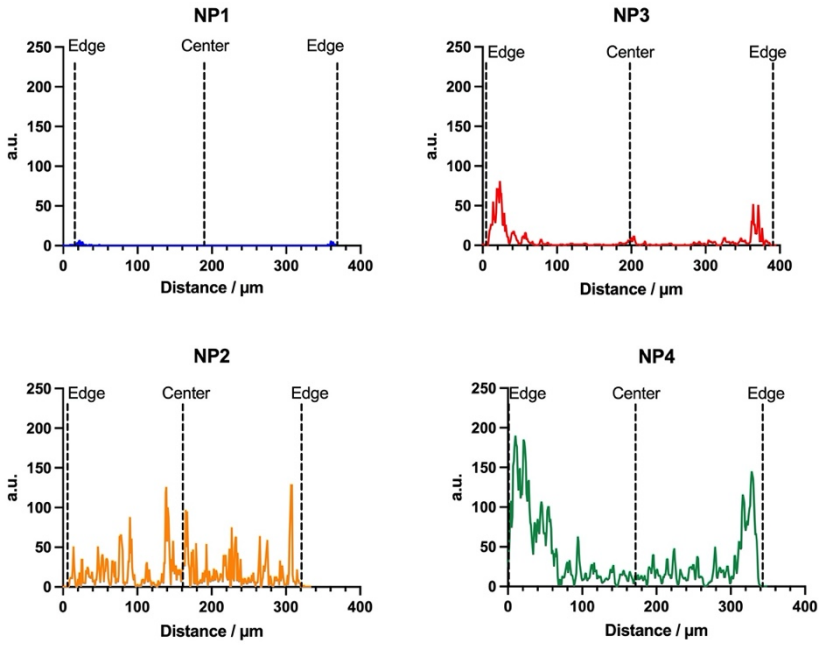

Figure S12. TT1 fluorescence intensity profiles passing through the equatorial plane section shown in Figure 3A.

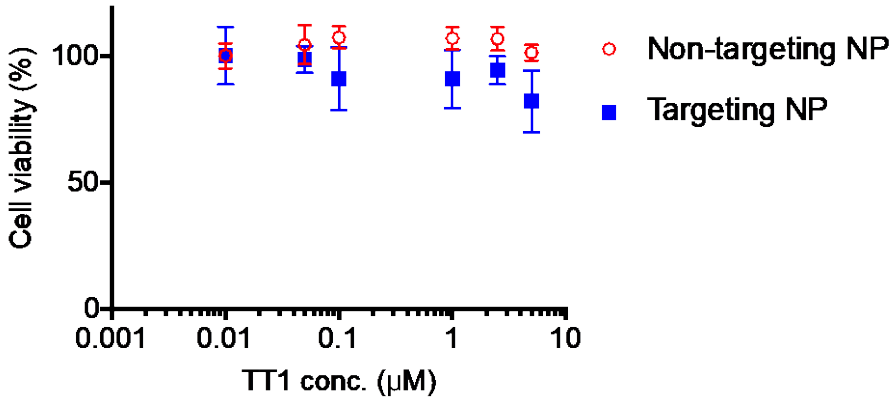

Figure S13. Dark toxicity of non-targeting or targeting NPs confirming the non-toxic nature of the NPs without light irradiation.

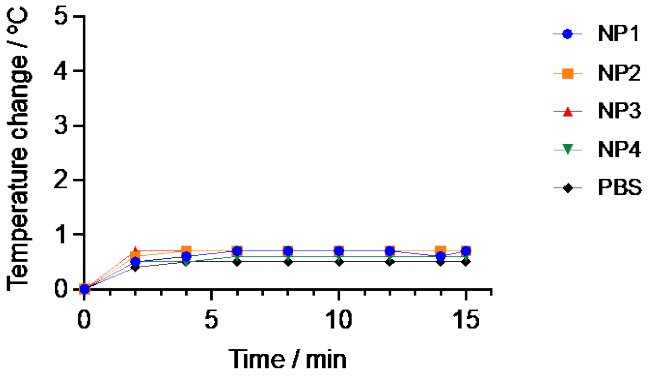

Figure S14. Temperature changes in TT1-loaded NP solutions during photo-irradiation. The data indicate effects from temperature increase are negligible.

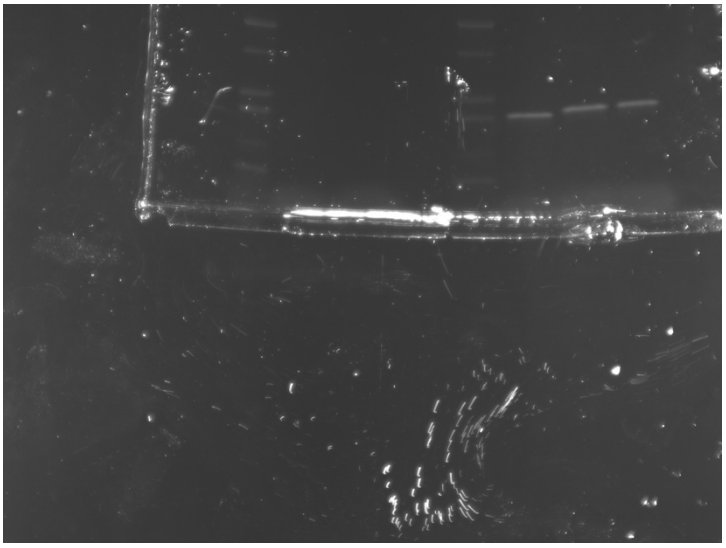

Figure S15. Uncropped gel for Figure 1C.

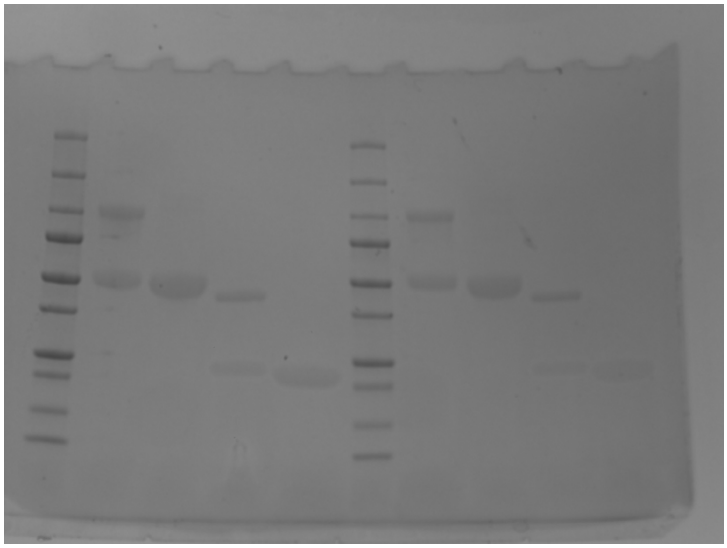

Figure S16. Uncropped gel for Figure S1.

Amino acid sequences of the ELPs

[A_3G_2-60]-[V_4F_1-50]

GAGVPGAGVPGAGVPGGGVPGGGVPGAGVPGAGVPGAGVPGGGVPGGGVPGAGVPGAGVPGAGVPGGGVPGGGVPGAGVPGA
GVPGAGVPGGGVPGGGVPGAGVPGAGVPGAGVPGGGVPGGGVPGAGVPGAGVPGAGVPGGGVPGGGVPGAGVPGAGVPGAGV
PGGGVPGGGVPGAGVPGAGVPGAGVPGGGVPGGGVPGAGVPGAGVPGAGVPGGGVPGGGVPGAGVPGAGVPGAGVPGGGVP
GGGVPGAGVPGAGVPGAGVPGGGVPGGGVPGAGVPGAGVPGAGVPGGGVPGGGVPGVGVPGVGVPGFGVPGVGVPGVGVPGV
GVPGVGVPGFGVPGVGVPGVGVPGVGVPGVGVPGFGVPGVGVPGVGVPGVGVPGVGVPGVGVPGVGVPGVGVPGVGVPGVGVP
GFGVPGVGVPGVGVPGVGVPGVGVPGFGVPGVGVPGVGVPGVGVPGVGVPGFGVPGVGVPGVGVPGVGVPGVGVPGFGVPGVG
VPGVGVPGVGVPGVGVPGFGVPGVGVPGVGVPGVGVPGVGVPGFGVPGVGVPGVGVPGW

7D12-[A_3G_2-60]-[V_4F_1-50]

QVKLEESGGGSVQTGGSLRLTCAASGRTSRSYGMGWFRQAPGKEREFVSGISWRGDSTGYADSVKGRFTISRDNAKNTVDLQMNS
LKPEDTAIYYCAAAAGSAWYGTLYEYDYWGQGTQVTVSAEPKTPKPQPAAGSGAGVPGAGVPGAGVPGGGVPGGGVPGAGVPGA
GVPGAGVPGGGVPGGGVPGAGVPGAGVPGAGVPGGGVPGGGVPGAGVPGAGVPGAGVPGGGVPGGGVPGAGVPGAGVPGAGV
PGGGVPGGGVPGAGVPGAGVPGAGVPGGGVPGGGVPGAGVPGAGVPGAGVPGGGVPGGGVPGAGVPGAGVPGAGVPGGGVP
GGGVPGAGVPGAGVPGAGVPGGGVPGGGVPGAGVPGAGVPGAGVPGGGVPGGGVPGAGVPGAGVPGAGVPGGGVPGGGVPG
AGVPGAGVPGAGVPGGGVPGGGVPGVGVPGVGVPGFGVPGVGVPGVGVPGVGVPGVGVPGFGVPGVGVPGVGVPGVGVPGVG
VPGFGVPGVGVPGVGVPGVGVPGVGVPGFGVPGVGVPGVGVPGVGVPGVGVPGVGVPGVGVPGVGVPGVGVPGFGVPGVGVPG
VGVPGVGVPGVGVPGVGVPGFGVPGVGVPGVGVPGVGVPGVGVPGFGVPGVGVPGVGVPGVGVPGVGVPGFGVPGVGVPGVGV
PGVGVPGVGVPGFGVPGVGVPGVGVPGW

mbELP [M_1V_3-40]

MWVPGVGVPGVGVPGMGVPGVGVPGVGVPGVGVPGMGVPGVGVPGVGVPGVGVPGMGVPGVGVPGVGVPGVGVPGMGVPGV
GVPGVGVPGVGVPGMGVPGVGVPGVGVPGVGVPGMGVPGVGVPGVGVPGVGVPGMGVPGVGVPGVGVPGVGVPGMGVPGVGV
PGVGVPGVGVPGMGVPGVGVPGVGVPGVGVPGMGVPGVG

References

[1] J. R. McDaniel, J. A. MacKay, F. G. Quiroz, A. Chilkoti, *Biomacromolecules* **2010**, *11*, 944–952.

[2] V. Ibrahimova, J. A. Gonzalez-Delgado, M. Leveque, T. Torres, E. Garanger, S. Lecommandoux, *Bioconjug. Chem.* **2021**, *32*, 1719–1728.

[3] J. Pille, S. A. M. van Lith, J. C. M. van Hest, W. P. J. Leenders, *Biomacromolecules* **2017**, *18*, 1302–1310.

[4] L. M. P. E. van Oppen, J. Pille, M. van Stevendaal, L. N. van der Vorm, J. A. M. Smeitink, W. J. H. Koopman, P. H. G. M. Willems, J. C. M. van Hest, R. Brock, *Eur. J. Pharm. Biopharm.* **2019**, *137*, 175–184.

[5] S. Bolte, F. P. Cordelieres *J Microsc.* **2006**, *224*, 213-232.

Author Contributions

D. H. T. L. designed and performed the experiments except others indicated. V. I. and E. G. prepared TT1-mbELP. H.-L. W. performed Cryo-TEM. A. F. and T. T. provided TT1-azide. D.H.T.L. and S. A. H. W. performed and analyzed Q-ToF LC/MS data. D.H.T.L. analyzed the data. D. H. T. L., B. R., W. P. J. L., J. C. M. v. H. wrote the manuscript. B. R., W. P. J. L., S. L., and J. C. M. v. H. conceived, designed, and oversaw the study. All authors read and approved the manuscript.